Available online at www.sciencedirect.com
SCIENCE DIRECT®
Journal of Sound and Vibration 285 (2005) 767–782
JOURNAL OF SOUND AND VIBRATION
www.elsevier.com/locate/jsvi

Detection of crack location and size in structures using wavelet finite element methods

B. Li*, X.F. Chen, J.X. Ma, Z.J. He

Automation School of Mechanical Engineering, Institute of Mechanical Engineering, Xi'an Jiaotong University, Xi'an 710049, People's Republic of China

Received 5 November 2003; received in revised form 15 March 2004; accepted 27 August 2004
Available online 22 December 2004

Abstract

A methodology to detect crack location and size is presented which takes advantage of wavelet finite element methods (WFEM) in the modal analysis for singularity problems like a cracked beam. First, the beam is discretized into a set of wavelet finite elements, and then the natural frequencies of the beam with various crack locations and sizes are accurately obtained. The frequency response functions, function of crack location and size, are approximated by means of surface-fitting techniques. Measured natural frequencies are used in a crack detection process and the crack location and size can be identified by finding the point of intersection of three frequency contour lines. The experimental data from a free–free beam studied by Silva are employed to verify the accuracy of the method. The present method is general and can be easily extended to complex structures with multiple cracks.
© 2004 Elsevier Ltd. All rights reserved.

1. Introduction

It is well known that cracks are a main cause of structural failure. The sudden failure of structural components is very costly and may be catastrophic in terms of human life and property damage. In order to reduce or even eliminate structural failure, it is desirable to detect cracks when they are still very small. Non-destructive testing methods, such as ultrasonic testing, X-ray,

*Corresponding author. Tel.: +86 29 8266 7963; fax: +86 29 8266 3689.
E-mail address: bli@mailst.xjtu.edu.cn (B. Li).

0022-460X/$ - see front matter © 2004 Elsevier Ltd. All rights reserved.
doi:10.1016/j.jsv.2004.08.040

acoustic emission, etc., are generally useful for this purpose. However, most of these methods are inconvenient in many situations due to the need for the investigator to have access to the component under analysis for crack detection [1]. This inconvenience can be avoided through the use of vibration-based inspection (VBI) because measurement and collection of vibration parameters like natural frequencies are easy. Additionally, VBI methods do not require the cleaning of local areas compared to others. The detection of defects through VBI can be applied to cracks far away from the sensors and to areas whose surfaces are not accessible. VBI methods are also cheap and quick [2].

Currently, these promising potentials for VBI methods have received much attention from mathematicians and engineers [3–9]. Various crack models and associated vibration-based methods have been presented. Rizos et al. [3] modeled the crack as a local flexibility and used an analytical method to relate the measured vibration modes to the crack location and size. Nandwana and Maiti [4], and Chaudhari and Maiti [5] represented the crack as a rotational spring and employed a semi-analytical method for detection of a crack location and depth in a cantilever beam. Meanwhile, there are more investigators who further employed finite element methods (FEM) for identification of crack in structures due to the fact that FEM become firmly established as a standard procedure for the solution of crack problems [6]. Chinchalkar [7] used variable depth finite elements with two nodes and two degrees of freedom per node for modeling a beam of varying depth, the location and size of crack are then detected. Ostachowicz and Krawczuk [8], and Lele and Maiti [9], respectively, employed triangular finite elements and eight-noded iso-parametric elements to make more efficient calculation for the crack detection. However, an extreme refined mesh in the crack region and a great amount of computational work in Refs. [6–9] are required due to the inherent defects that the traditional finite elements are impotent to describe the singular behavior of cracks [10].

In order to overcome the difficulties that traditional FEM have, wavelet spaces have been employed as approximate spaces and then wavelet finite element methods (WFEM) have been derived [11–19]. By comparison with the conventional FEM, WFEM lend several advantages for modal analysis of crack problems. A main attractive feature is that WFEM have the ability to accurately represent fairly general functions with a small number of wavelet coefficients, as well as to characterize the smoothness of such functions from the numerical behavior of these coefficients [12]. Furthermore, since the condition numbers of WFEM is independent of mesh size, which was proved by Jaffard and Laurencot [13], WFEM can avoid numerical instability that traditional FEM exist in the analysis for the crack problems. In addition, when orthogonal Daubechies wavelet functions with compact support are employed as interpolation functions, the stiffness matrixes that WFEM generate are sparse, which can greatly shorten computational work.

In the present paper, a simple methodology to detect crack location and size is presented, which takes full advantages of WFEM in modal analysis for singularity problems like a cracked beam. The procedure of crack detection based on WFEM is described. Firstly, the first three natural frequencies of the beam with various crack locations and sizes are accurately found by means of WFEM. The frequency response function (FRF) [20], as a function of crack location and size, is approximated through surface-fitting techniques and three-dimensional plots of FRFs are shown. Then, for a particular crack location and size, the three frequency contour lines of the beam are obtained under the situation that measured natural frequencies of crack beams are set as input. The crack location and size can be identified through finding the points of intersection of the three

contour lines. A free–free beam by Silva and Gomes [1] is employed to verify the accuracy of the current crack detection method.

2. Wavelet finite element analysis

2.1. Wavelet-based finite elements

The basic idea of WFEM, which is similar to the traditional FEM, is to discretize a body into an assemble of discrete finite elements which are interconnected at the nodal points on element boundaries. The displacement field is approximated over each wavelet-based finite element, in terms of the nodal displacements. Ma et al. [18] have constructed one-dimensional Daubechies wavelet-based beam elements for the beam bending problems. Chen et al. [19] have presented two-dimensional wavelet finite elements based on Daubechies wavelets and applied them to the plane-stress and plane-strain problems. For completeness, the forms of the derivation of wavelet-based element equations are given here.

For a one-dimensional wavelet-based finite element, the nodal displacements can be represented by the shape functions, whose forms are as follows:

$$\mathbf{N} = \boldsymbol{\varphi}\mathbf{T}, \tag{1}$$

where $\mathbf{T}$ stands for the transform matrix, and its elements t_{ij} are given in the appendix. φ denotes the Daubechies wavelet scaling function collection, which value can be found in Ref. [21]. While for an arbitrary two-dimensional wavelet-based finite element, the shape functions are given as

$$\mathbf{N} = \mathbf{N}_x \otimes \mathbf{N}_y, \tag{2}$$

where $\otimes$ is Kronecker symbol, $\mathbf{N}_x$ ($=[N_{x,1},\ldots,N_{x,i},\ldots,N_{x,n}]$) and $\mathbf{N}_y$ ($=[N_{y,1},\ldots,N_{y,i},\ldots,N_{y,n}]$) are the shape functions in the horizontal (x) and vertical (y) directions, respectively.

After constructing wavelet-based shape functions, the procedures of construction of the stiffness matrix $\mathbf{K}_e$ and the mass matrix $\mathbf{M}_e$ can be achieved as in the traditional FEM. The forms of both matrixes are represented as

$$\mathbf{K}_e = \int_{\Omega} (\mathbf{LN})^{\mathrm{T}} \mathbf{D} (\mathbf{LN}) d_x d_y, \tag{3}$$

$$\mathbf{M}_e = \int_{\Omega} \rho \mathbf{N}^{\mathrm{T}} \mathbf{N} d_x d_y, \tag{4}$$

where $\mathbf{L}$ and $\mathbf{D}$ denote the generalized strain and the elasticity matrix, respectively. ρ is the beam density. The superscript T stands for the transpose of a matrix or a vector.

2.2. Modal analysis of a cracked beam

A uniform beam with an open crack located at $\beta = e/L$ is shown in Fig. 1. L, H, and B represent the length, height and width of the beam, respectively. e and a are the crack location and crack size, respectively. β and α stand for the normalized crack position and normalized crack size, respectively.

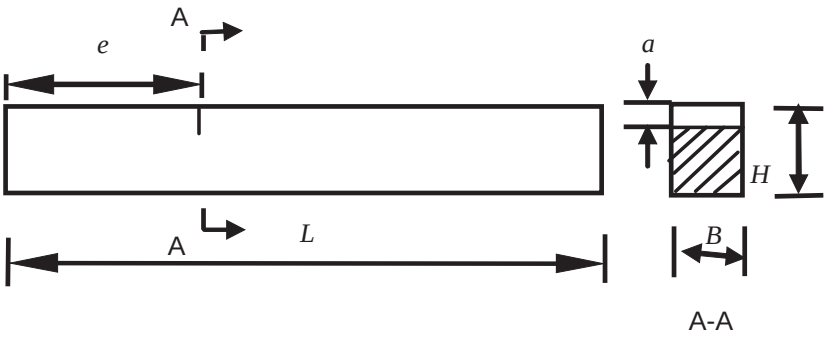

Fig. 1. The modal of free–free beam with an open crack.

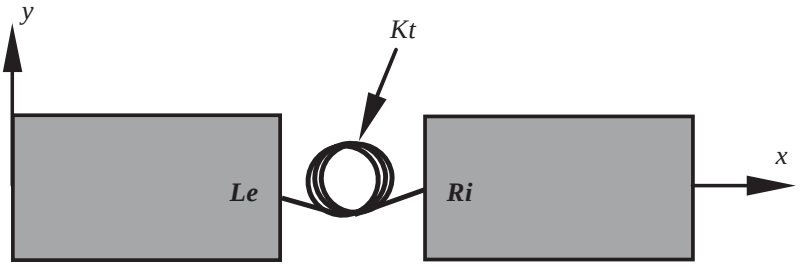

Fig. 2. Wavelet-based beam element with an open crack simulated by elastic element.

Suppose that the crack is located between two wavelet-based finite elements, and the numbers of two nodes are Le and Ri, respectively (see Fig. 2). The crack introduces a local flexibility that is a function of the crack depth, the flexibility changes the stiffness of the beam. Rizos et al. [22] represented the crack by a massless rotational spring with a computable stiffness Kt. The values of Kt for the various cross sections were given by Dimarogonas [23]. The continuity conditions at the crack position indicate that the left and right nodes have the same vertical deflection, $y_{\mathrm{Le}} = y_{\mathrm{Ri}}$, while their rotations θ_{Le} and θ_{Ri} are connected through the stiffness matrix $\mathbf{K}_c$ [7]

$$\mathbf{K}_c = \begin{bmatrix} Kt & -Kt \\ -Kt & Kt \end{bmatrix}. \tag{5}$$

Hence, we can assemble $\mathbf{K}_c$ into the global stiffness matrix, $\mathbf{K}$, through employing a single dof of the vertical deflection of both nodes Le and Ri. The global mass matrix of cracked beam is equal to the uncracked.

Using the displacement-based formulation in conjunction with the principle of virtual displacement, the equations of the beam motion can be then written as

$$\mathbf{M}\ddot{\mathbf{Y}} + \mathbf{K}\mathbf{Y} = 0, \tag{6}$$

where overdots indicate differentiation with respect to time, $\mathbf{M}$ and $\mathbf{K}$ are the global mass and stiffness matrix, respectively. $\mathbf{Y}$ $(= [y_1, \theta_1, \ldots y_n, \theta_n])$ is the column vector of nodal displacements.

Supposing that a time harmonic solution for the nodal displacements can be represented as

$$\mathbf{Y} = \mathbf{A} \sin \omega_i t, \tag{7}$$

where $\mathbf{A}$ is the amplitude of the nodal displacements. Substituting Eq. (7) into Eq. (6) leads to

$$[-\omega_i^2 \mathbf{M} + \mathbf{K}]\{\mathbf{A}\} = 0. \tag{8}$$

For non-trivial solutions,

$$\det(\mathbf{K} - \omega_i^2 \mathbf{M}) = 0, \tag{9}$$

where "det" denotes the determinant and ω_i is the natural frequency. Therefore, the effective values of the natural frequencies can be found through solving generalized eigenvalues of Eq. (9).

3. Crack identification methods

Based on the calculated first three natural frequencies, FRFs are approximated using surface-fitting techniques. Since the crack location and the crack size influence the changes in the natural frequencies of a cracked beam, a particular frequency can correspond to different crack locations and crack sizes. This can be observed from three-dimensional plots of the first three natural frequencies of the free–free beam. On this basis, a contour line, which has the same frequency resulting from a combination of different crack locations and crack sizes (for a particular mode) can be plotted in a curve with crack position and crack size as its axes [24].

For illustrative purposes, the three-dimensional contour lines for the first three natural frequencies for a particular crack case (as listed in Table 1) are plotted in Fig. 3.

Table 1
Damage scenarios and resonance frequencies (Hz) of free–free beams [1]

Crack Case	Actual crack		Mode 1		Mode 2		Mode 3	
	Location β	Size α	Uncracked	Cracked	Uncracked	Cracked	Uncracked	Cracked
1	0.125	0.125	315.9	316.0	860.2	859.4	1654.5	1649.0
2	0.125	0.250	316.3	316.1	862.6	857.8	1659.0	1632.5
3	0.125	0.375	317.6	316.6	864.8	851.4	1663.0	1593.5
4	0.125	0.500	314.7	313.0	856.8	826.6	1647.0	1515.0
5	0.250	0.125	316.8	315.9	861.6	855.2	1657.5	1647.5
6	0.250	0.250	317.7	314.1	864.4	840.6	1662.0	1626.5
7	0.250	0.375	317.8	308.8	864.8	805.2	1662.5	1580.5
8	0.250	0.500	323.8	305.4	878.8	870.4	1689.5	1534.0
9	0.375	0.125	313.5	311.7	855.0	853.8	1646.0	1646.5
10	0.375	0.250	315.4	307.1	858.6	842.4	1653.0	1651.5
11	0.375	0.375	316.6	296.2	862.4	825.0	1659.5	1655.5
12	0.375	0.500	328.8	279.0	873.4	805.2	1679.5	1672.0
13	0.500	0.125	316.7	313.0	862.8	863.2	1658.0	1645.5
14	0.500	0.250	315.6	303.0	859.4	859.8	1652.0	1606.5
15	0.500	0.375	317.8	291.5	865.8	866.0	1664.5	1574.0
16	0.500	0.500	320.6	265.1	873.0	873.2	1678.0	1498.0

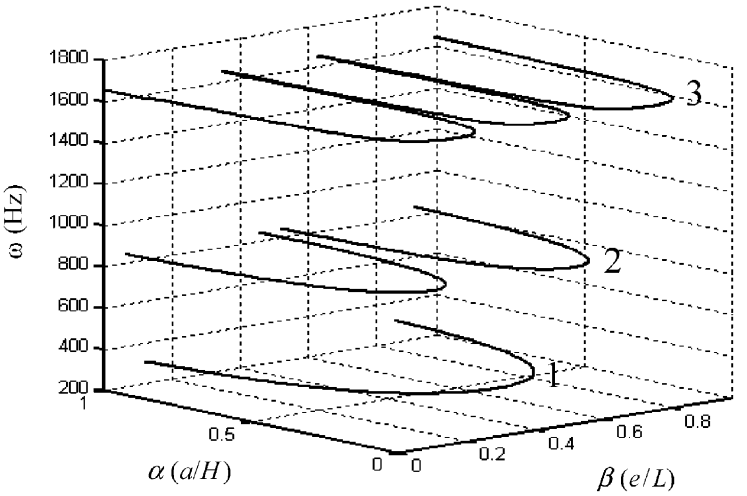

Fig. 3. Three-dimensional plots of the frequency contour lines for a free–free beam [1] (1: mode 1; 2: mode 2; and 3: mode 3).

The development of a crack, at a certain location, corresponds to a sudden reduction of the bending stiffness of the beam, and furthermore leads to a shift of the natural frequency. The inverse problem of the crack identification is to predict the location β and depth α of a crack once the value of natural frequencies ω_i is measured, i.e.,

$$(\alpha, \beta) = g_i(\omega_i). \tag{10}$$

The measurements of any two natural frequency variations ω_1 and ω_2 enable one to define the location and depth of a crack if the function $g_i(\omega_i)$ is known [1]. If the crack coincides the vibration node of one mode, the frequency for that mode remains almost unchanged. Therefore a minimum of three curves is required to identify the two unknown parameters of crack location and size.

4. Experimental verification

4.1. Description of test structure

The crack detection methods are validated using a comprehensive data provided by Silva and Gomes [1]. Those researchers performed an extensive set of modal analysis experiments on free–free uniform beams with the goal of providing objective data to validate proposed techniques for damage detection. Kim and Stubbs [25] used those data to assess the accuracy of their crack detection method.

Test specimens in Ref. [1] were steel beams with $0.032 \times 0.016\,\mathrm{m}^2$ rectangular cross-section and 0.72 m long. The corresponding material properties were: $E = 206\,\mathrm{GPa}$, $\nu = 0.29$, and $\rho = 7650\,\mathrm{kg/m}^3$. Here the results of 32 experiments reported by Silva and Gomes [1] are utilized:

16 experiments on uncracked beams and corresponding 16 experiments on cracked beams. The following procedures were utilized for the experiments. The first four bending frequencies were measured for each of 16 uncracked free–free beams. Then a cut was introduced into each beam and the same four bending frequencies were measured. The crack in each beam was simulated by a cut normal to the beams' longitudinal axis, with a controlled depth (as listed in Table 1). In order to avoid the nonlinear characteristics of an opening and closing crack, the thickness of the cut was carefully defined, taking into account that both sides of the crack were not supposed to make contact during the dynamic bending of the beam.

Table 1 presents the total 16 damage scenarios that include four different crack-locations and four crack-size levels at each location. The two sets of bending frequencies measured before and after the damage episodes are also listed in Table 1.

4.2. Crack identification practice

4.2.1. Correction of Young's modulus

The evaluation of the natural frequencies through the characteristic equation (9) of the free–free beams requires the knowledge of the material properties. Quoted values of Young's modulus are not sufficiently accurate for this purpose. The problem can be overcome by an iterative approach, which uses the undamaged natural frequencies of the beams to determine an effective value of the Young's modulus [26]. The procedures of the iterative approach are as follows.

Taking the measured undamaged beam natural frequencies ω_i by Silva and Gomes [1] as input parameters, the characteristic equation (9) can be written in the following form:

$$\det\left(\omega_i^2\mathbf{M} - E_m\frac{\mathbf{K}}{E}\right) = 0, \tag{11}$$

where E_m is the corrected value of Young's modulus E. The value of E_m for each mode can be found through solving the generalized eigenvalues of the matrixes $\omega_i^2\mathbf{M}$ and $\mathbf{K}/E$. The values of E_m for different crack cases (as listed in Table 1) are given in Table 2.

It should be noted that the physical significance for the correction of Young's modulus E is not to change the value E, but to narrow the error between the numerical model and real-life situation. In fact, this is a zero setting procedure. In order to make the numerical undamaged frequencies for different mode be equal to the measured values, effective values of Young's modulus must be found for each mode.

4.2.2. Evaluation of natural frequencies

In order to obtain natural frequencies with high accuracy, the wavelet finite element analysis is performed. Substituting the Young's modulus in Eq. (9) with the corrected one of a certain crack case in Table 2, the first three natural frequencies of the free–free beam with an arbitrary crack position and size can be found through solving the characteristic equation (9). We correct E_m for each mode by employing eight wavelet-based finite elements, D6 [18] and calculate the natural frequencies of the free–free cracked beam. In order to make a comparison with the traditional FEM, we also evaluate the frequencies by using 40 Beam3 elements [27] of FEM. The values of natural frequencies by WFEM and FEM are tabulated in Table 3, respectively. Obviously, employing fewer wavelet-based finite elements can obtain higher analytical accuracy.

Table 2
The corrected values of Young's modulus for different crack cases [1]

Crack case	E_m (Gpa)		
	Mode 1	Mode 2	Mode 3
1	1.8961	1.8502	1.7809
2	1.9010	1.8606	1.7906
3	1.9166	1.8692	1.7993
4	1.8818	1.8356	1.7648
5	1.9070	1.8563	1.7874
6	1.9178	1.8683	1.7971
7	1.9190	1.8701	1.7982
8	1.9922	1.9311	1.8571
9	1.8674	1.8279	1.7627
10	1.8902	1.8434	1.7777
11	1.9046	1.8597	1.7917
12	2.0542	1.9075	1.8351
13	1.9058	1.8614	1.7885
14	1.8925	1.8468	1.7755
15	1.9190	1.8744	1.8025
16	1.9530	1.9057	1.8319

Table 3
Comparison of the values of natural frequencies between WFEM and FEM for different crack cases listed in Table 1

Crack Case	Natural frequencies (Hz)					
	WFEM (Error %)			FEM (Error %)		
	Mode 1	Mode 2	Mode 3	Mode 1	Mode 2	Mode 3
1	315.8(0.06)	859.0(0.05)	1648.9(0.01)	315.8(0.06)	860.6(0.14)	1657.3(0.50)
2	316.0(0.03)	857.9(0.01)	1636.6(0.25)	316.0(0.03)	859.4(0.19)	1644.5(0.74)
3	316.8(0.06)	852.8(0.16)	1607.7(0.89)	316.8(0.06)	854.2(0.33)	1614.5(1.32)
4	313.1(0.03)	833.1(0.79)	1539.1(1.59)	313.1(0.03)	834.3(0.93)	1544.0(1.91)
5	316.0(0.03)	855.8(0.07)	1648.0(0.03)	316.0(0.03)	857.4(0.26)	1656.5(0.55)
6	314.5(0.13)	842.0(0.17)	1627.1(0.04)	314.5(0.13)	843.4(0.32)	1635.1(0.53)
7	310.2(0.45)	813.4(1.02)	1588.2(0.49)	310.2(0.45)	814.5(1.15)	1595.6(0.96)
8	307.7(0.75)	866.3(0.47)	1563.2(1.90)	307.7(0.75)	782.0(10.16)	1570.0(2.35)
9	311.5(0.06)	851.0(0.33)	1645.6(0.05)	311.5(0.06)	852.5(0.15)	1654.2(0.47)
10	307.7(0.20)	843.4(0.12)	1651.7(0.01)	307.7(0.20)	844.9(0.30)	1660.2(0.53)
11	298.4(0.74)	828.4(0.41)	1656.5(0.06)	298.4(0.74)	844.9(0.58)	1665.0(0.03)
12	290.9(4.27)	812.8(0.94)	1674.1(0.13)	290.9(4.27)	814.0(1.09)	1682.5(0.63)
13	314.0(0.32)	862.8(0.05)	1647.9(0.15)	315.0(0.64)	839.7(2.72)	1552.9(5.63)
14	305.6(0.86)	859.4(0.05)	1615.1(0.54)	305.6(0.86)	861.0(0.14)	1622.7(1.01)
15	294.5(1.03)	865.8(0.02)	1582.1(0.51)	294.5(1.03)	867.4(0.16)	1588.7(0.93)
16	277.0(4.49)	873.0(0.02)	1534.8(2.46)	276.9(4.45)	874.6(0.16)	1540.1(2.81)

Taking the beam of crack case 10 as an example, the FRFs are plotted for the three modes in Fig. 4. Fig. 5 shows the plots of the variations of the first three natural frequencies as a function of crack size for some of the crack locations of a free–free beam [1]. Fig. 6 illustrates the variations of the first three natural frequencies as a function of crack location.

4.2.3. Detection of crack location and crack size

The method for crack identification is verified for several combinations of crack positions and crack sizes listed in Table 1. The first three natural frequencies measured by Silva and Gomes [1] are used as input in this case. The variation of crack size α and crack position β with E correction are plotted for the three modes in Fig. 7. The intersection of the three curves indicates the possible crack position and crack size. When the three curves do not meet exactly, the centroid [9] of the three pairs of intersections is taken as the crack position and crack size. The predicted crack positions and crack sizes for two set of Young's modulus are compared with the corresponding actual values and the results are presented in Tables 4 and 5, respectively.

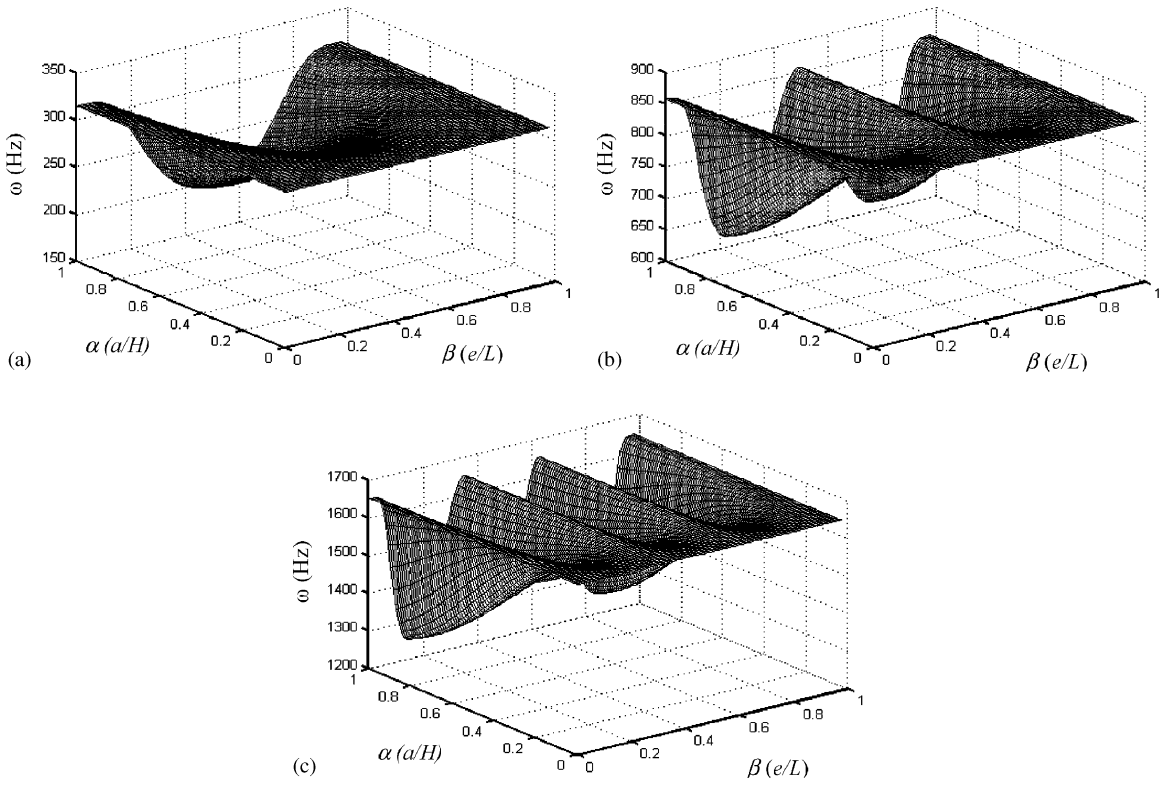

Fig. 4. Three-dimensional plots of natural frequency versus crack position, and crack size for a free–free beam [1]: (a) mode 1; (b) mode 2; and (c) mode 3.

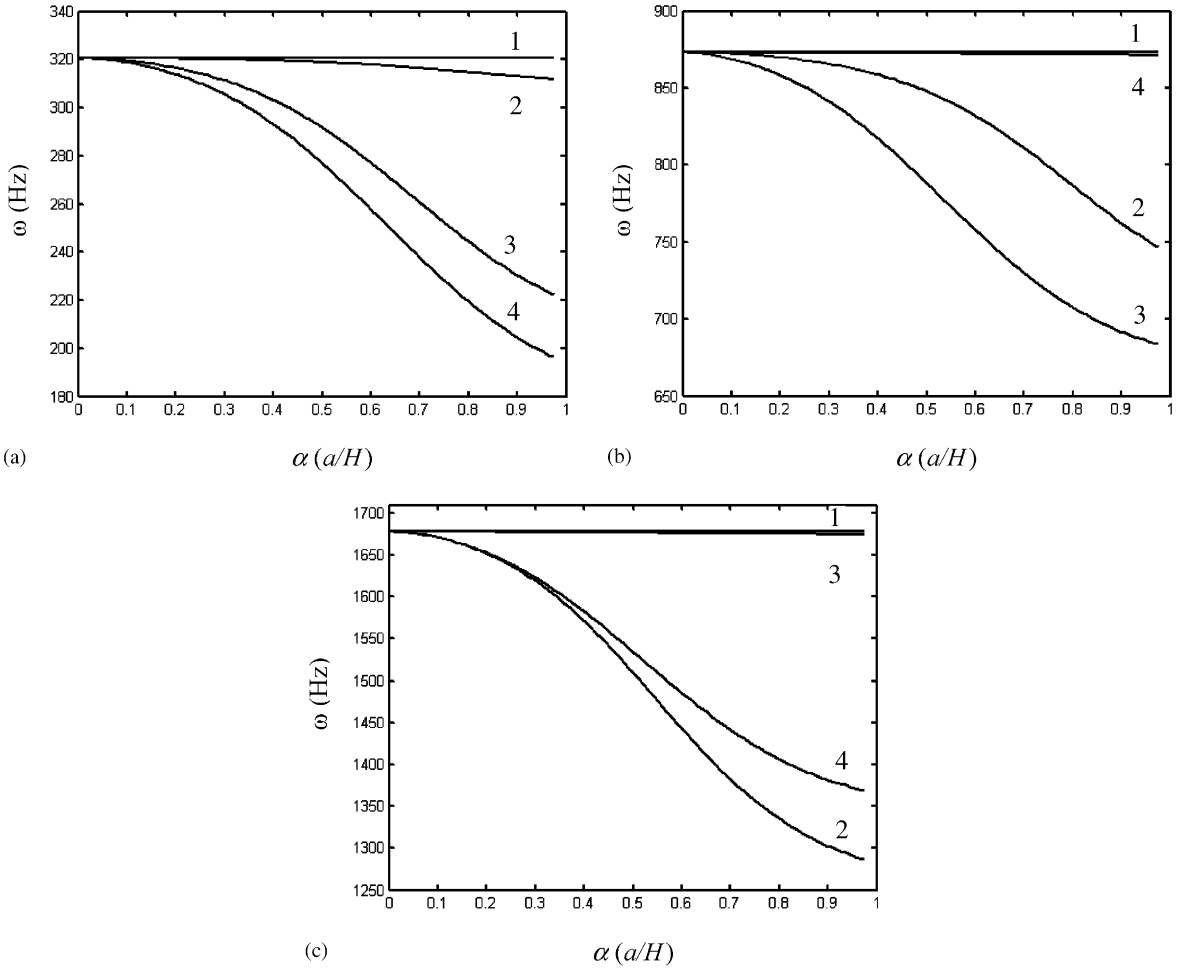

Fig. 5. Natural frequencies of various modes in terms of crack size for a free–free beam [1] (1: uncracked; 2: $\beta = \frac{1}{8}$; 3: $\beta = \frac{1}{3}$; and 4: $\beta = \frac{1}{2}$): (a) mode 1; (b) mode 2; (c) mode 3).

4.2.4. Assessment of crack identification results

From the experimental results and plots, the following assessments are made for all the crack cases considered:

(1) For all the cases considered, the natural frequencies decrease when the crack sizes increase. While for a few of the considered, the frequencies remained unchanged until a certain value of crack size ratio is attained, after which, the frequencies decreases rapidly. For larger values of crack size ratio, the frequency decreases rapidly (see Fig. 5).

(2) When the crack is located at the center of the beam, the second natural frequency is almost unaffected. While the crack is located at the position of $\beta = \frac{1}{3}$ (or $\beta = \frac{2}{3}$), the third natural frequency is almost unaffected. This is due to the fact that those natural frequencies are insensitive to the crack existence because it is located at the node of those two modes of vibration (see Figs. 5 and 6).

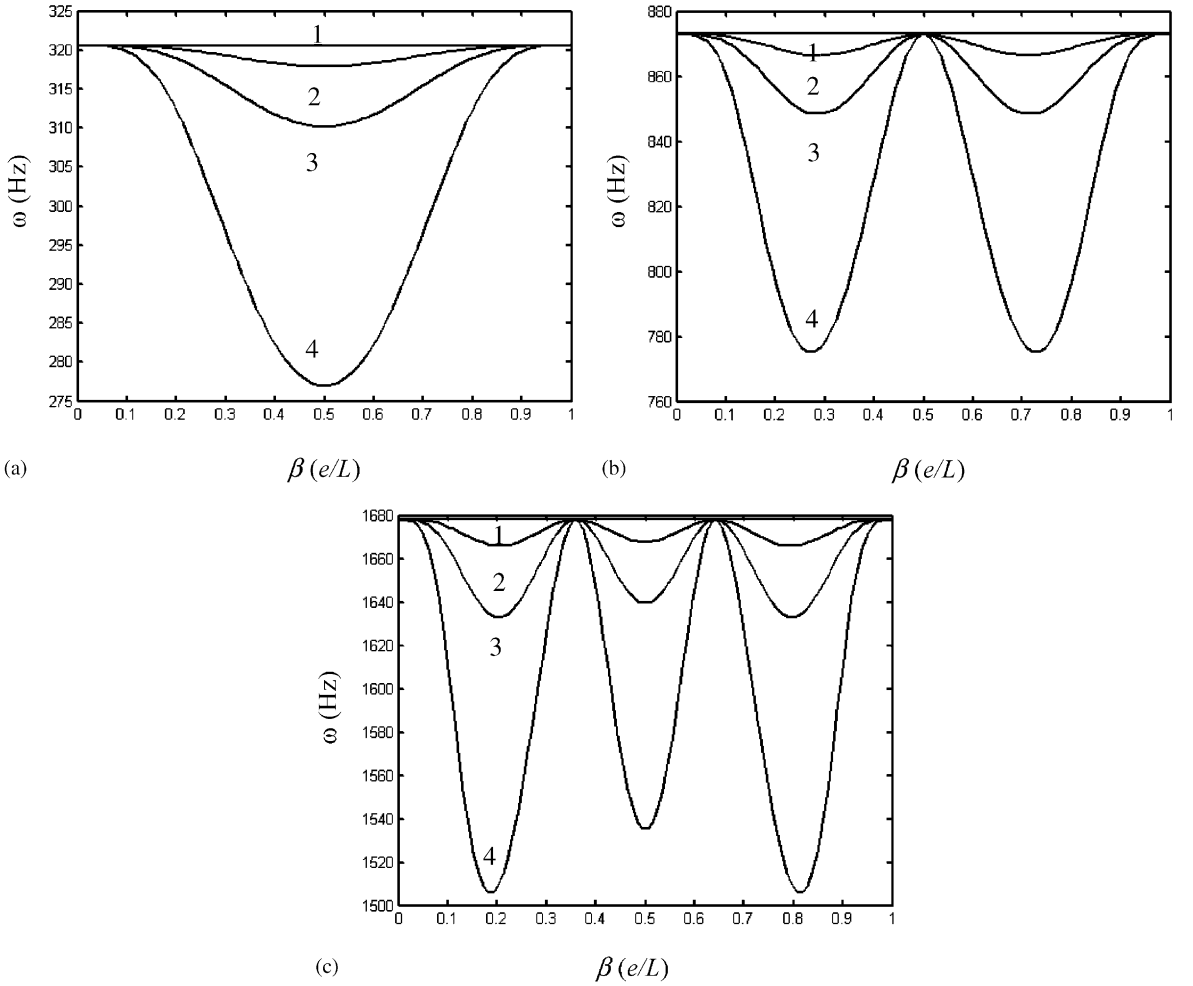

Fig. 6. Natural frequencies of various modes in terms of crack location for a free–free beam [1] (1: uncracked; 2: $\alpha = \frac{1}{8}$; 3: $\alpha = \frac{1}{4}$; and 4: $\alpha = \frac{1}{2}$): (a) mode 1; (b) mode 2; (c) mode 3).

(3) The predicted crack positions and crack sizes are in good agreement with the actual values. The average error of crack locations without E correction is 11.64 percent. While the average error of crack locations with E correction is 2.65 percent. The average error of crack sizes without E correction is 22.10 percent. While the average error of crack sizes with E correction is 5.62 percent (see Fig. 7).

5. Conclusions

A methodology based on WFEM to detect crack location and size is presented in this paper. The need for adequate data for an accurate description of dynamic influence of cracks is well satisfied. Through an approach for Young's modulus correction, the error between theoretical

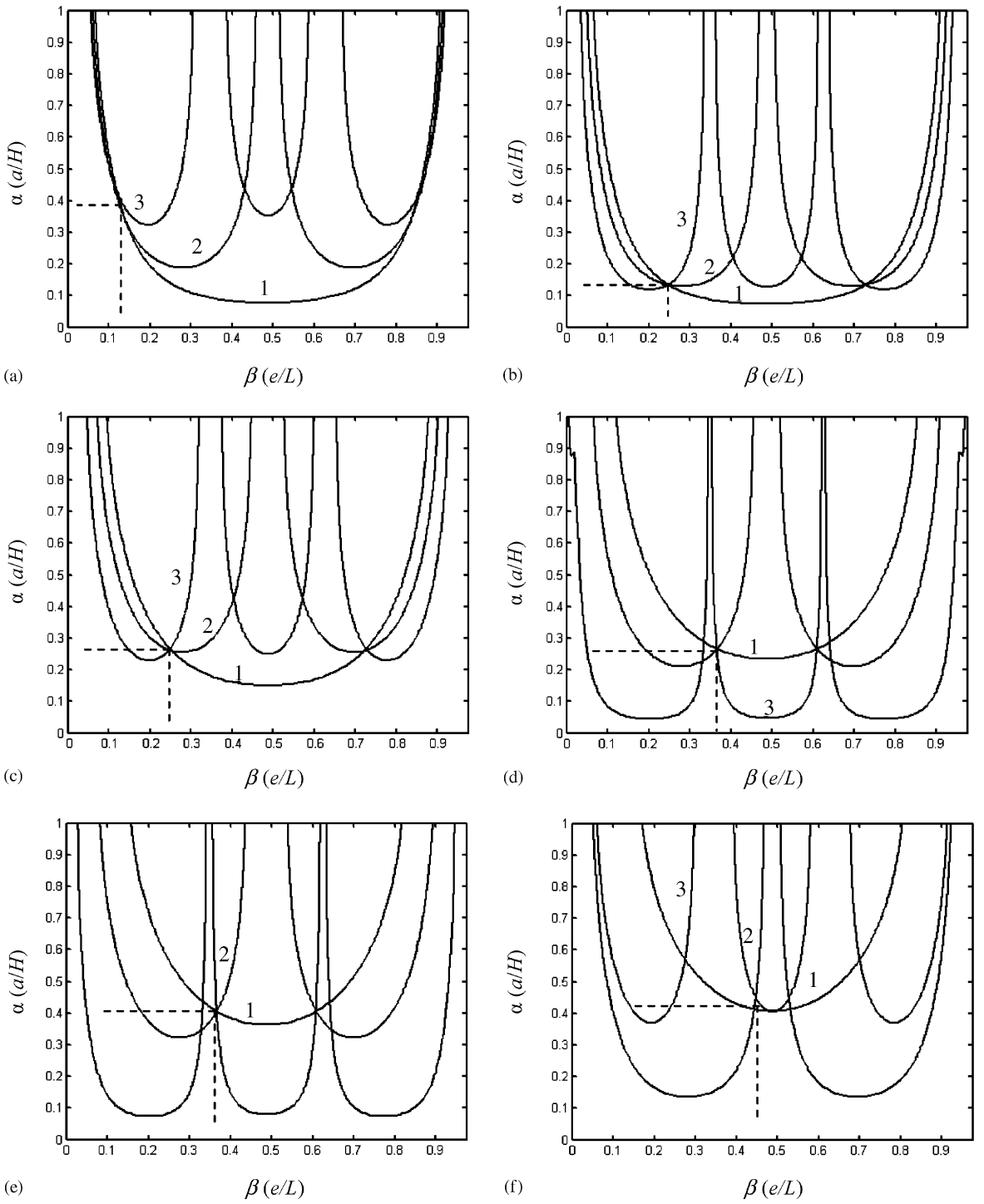

Fig. 7. Crack identification results with E correction by using the contour lines of the first three modes of a free–free beam [1] (1: mode 1; 2: mode 2; and 3: mode 3): (a) crack case 3; (b) crack case 5; (c) crack case 6; (d) crack case 10; (e) crack case 11; (f) crack case 15.

Table 4
Crack prediction and accuracy assessment results of test beams without E correction

Crack case	Actual crack		Predicted crack		Prediction accuracy	
	Location β	Size α	Location β	Size α	Locating error %	Sizing error %
1	0.125	0.125	0.244	0.386	11.9	26.1
2	0.125	0.250	0.225	0.423	10.0	17.3
3	0.125	0.375	0.211	0.470	8.6	9.5
4	0.125	0.500	0.212	0.555	8.7	5.5
5	0.250	0.125	0.248	0.424	0.2	29.9
6	0.250	0.250	0.243	0.465	0.7	21.5
7	0.250	0.375	0.235	0.550	1.5	17.5
8	0.250	0.500	0.225	0.655	2.5	15.5
9	0.375	0.125	0.250	0.450	12.5	32.5
10	0.375	0.250	0.265	0.471	11.0	22.1
11	0.375	0.375	0.282	0.525	9.3	15.0
12	0.375	0.500	0.292	0.600	8.3	22.5
13	0.500	0.125	0.251	0.432	24.9	30.7
14	0.500	0.250	0.252	0.525	24.8	27.5
15	0.500	0.375	0.235	0.630	26.5	25.5
16	0.500	0.500	0.252	0.850	24.8	35.0

Table 5
Crack prediction and accuracy assessment results of test beams with E correction

Crack case	Actual crack		Predicted crack		Prediction accuracy	
	Location β	Size α	Location β	Size α	Locating error %	Sizing error %
1	0.125	0.125	0.026	0.115	9.9	1.0
2	0.125	0.250	0.092	0.390	3.3	14.0
3	0.125	0.375	0.118	0.431	0.7	5.6
4	0.125	0.500	0.105	0.650	2.0	15.0
5	0.250	0.125	0.247	0.135	0.3	1.0
6	0.250	0.250	0.249	0.263	0.1	1.3
7	0.250	0.375	0.245	0.411	0.5	3.6
8	0.250	0.500	0.256	0.470	0.6	3.0
9	0.375	0.125	0.362	0.191	1.3	6.6
10	0.375	0.250	0.366	0.266	0.9	1.6
11	0.375	0.375	0.366	0.406	0.9	3.1
12	0.375	0.500	0.369	0.570	0.6	7.0
13	0.500	0.125	0.420	0.185	8.0	6.0
14	0.500	0.250	0.431	0.326	6.9	7.6
15	0.500	0.375	0.454	0.425	4.6	5.0
16	0.500	0.500	0.482	0.585	1.8	8.5

analysis and experimental studies, which are caused by boundary condition and material parameters, can be greatly reduced. Experimental results verify that the present method can be utilized to detect crack location as well as crack size. The procedure for detection of crack is

simple and general. It is believed that this procedure can be easily extended to complex structures, such as rotor, blade, etc. with multiple cracks.

Acknowledgements

This work is supported by National Natural Science Foundation of China (No. 50335030).

Appendix A

A.1. Transform matrix

In the case of wavelet finite element, the transform matrix possesses the form

$$\mathbf{T} = \mathrm{inv}(\mathbf{R}),$$

$$\mathbf{R} = \begin{bmatrix} \phi(10) & \phi(9) & \cdots & \phi(1) & \phi(0) \\ \phi\left(10+\frac{1}{8}\right) & \phi\left(9+\frac{1}{8}\right) & \cdots & \phi\left(1+\frac{1}{8}\right) & \phi\left(\frac{1}{8}\right) \\ \phi\left(10+\frac{2}{8}\right) & \phi\left(9+\frac{2}{8}\right) & \cdots & \phi\left(1+\frac{2}{8}\right) & \phi\left(\frac{2}{8}\right) \\ \phi\left(10+\frac{3}{8}\right) & \phi\left(9+\frac{3}{8}\right) & \cdots & \phi\left(1+\frac{3}{8}\right) & \phi\left(\frac{3}{8}\right) \\ \phi\left(10+\frac{7}{16}\right) & \phi\left(9+\frac{7}{16}\right) & \cdots & \phi\left(1+\frac{7}{16}\right) & \phi\left(\frac{7}{16}\right) \\ \phi\left(10+\frac{4}{8}\right) & \phi\left(9+\frac{4}{8}\right) & \cdots & \phi\left(1+\frac{4}{8}\right) & \phi\left(\frac{4}{8}\right) \\ \phi\left(10+\frac{9}{16}\right) & \phi\left(9+\frac{9}{16}\right) & \cdots & \phi\left(1+\frac{9}{16}\right) & \phi\left(\frac{9}{16}\right) \\ \phi\left(10+\frac{5}{8}\right) & \phi\left(9+\frac{5}{8}\right) & \cdots & \phi\left(1+\frac{5}{8}\right) & \phi\left(\frac{5}{8}\right) \\ \phi\left(10+\frac{6}{8}\right) & \phi\left(9+\frac{6}{8}\right) & \cdots & \phi\left(1+\frac{6}{8}\right) & \phi\left(\frac{6}{8}\right) \\ \phi\left(10+\frac{7}{8}\right) & \phi\left(9+\frac{7}{8}\right) & \cdots & \phi\left(1+\frac{7}{8}\right) & \phi\left(\frac{7}{8}\right) \\ \phi(11) & \phi(10) & \cdots & \phi(2) & \phi(1) \end{bmatrix},$$

where ‘inv’ denotes the inverse, the elements of the transform matrix **T** are tabulated in Table 6.

Table 6
$t_{i,j}$ for Daubechies wavelet of order 6

i/j	1	2	3	4	5	6	7	8	9	10	11
1	9.6730e7	−4.7223e8	7.0763e8	1.8808e9	−6.9991e9	8.1211e9	−4.2294e9	8.5056e8	1.3025e8	−1.1513e8	2.8931e7
2	8.0637e5	1.5206e6	−1.3247e7	−1.3709e7	9.5422e7	−3.6235e7	−1.8468e8	1.4254e8	−3.5541e7	1.1240e7	−1.2763e6
3	4.0848e5	8.0441e5	−7.1183e6	−3.1970e6	3.8597e7	−8.9262e6	−8.2605e7	7.0671e7	−2.6590e7	7.2681e6	−1.3898e6
4	1.9367e5	3.8212e5	−3.3625e6	−1.5489e6	1.9173e7	−4.0500e6	−3.1513e7	3.2622e7	−1.1621e7	3.5497e6	−5.0396e5
5	8.0571e4	1.5947e5	−1.3962e6	−6.1289e5	7.5846e6	−1.0095e6	−1.3018e7	1.5223e7	−4.7111e6	1.0291e6	−2.0835e5
6	2.7860e4	5.5385e4	−4.8081e5	−2.0106e5	2.3710e6	−5.7012e5	−5.2425e6	5.6096e6	−1.2173e6	4.6108e5	−8.5670e4
7	7.2667e3	1.4550e4	−1.2451e5	−4.8024e5	6.8714e5	−1.2684e5	−1.6027e6	1.9444e6	−4.5458e5	1.7260e5	−2.2879e4
8	1.1834e3	2.4004e3	−1.9910e4	−7.1480e3	1.4485e5	−1.7387e4	−2.2935e5	2.3554e5	−6.1558e3	2.6490e4	−3.8249e3
9	8.3050e1	1.7267e2	−1.3225e3	−5.6527e2	7.3957e3	−1.8417e3	−1.9847e4	1.6205e4	−4.1947e3	1.8343e3	−2.2176e2
10	−1.9500e0	−3.2073e0	3.9407e1	4.2576e1	−3.3922e2	1.9876e2	4.9799e2	−3.6429e2	9.9235e1	−2.0331e1	5.5849e0
11	1.0423e1	1.9443e1	−1.8477e2	−1.5910e1	1.8885e3	−4.6339e2	−2.1640e3	1.0971e3	−5.2378e2	1.4180e2	−2.8157e1

References

[1] J.M. Silva, A.J.L. Gomes, Experimental dynamic analysis of cracked free–free beams, *Experimental Mechanics* 30 (1) (1990) 20–25.

[2] X.F. Yang, Vibration Based Crack Analysis and Detection in Beams Using Energy Method, PhD Thesis, Faculty of Engineering and Applied Science Memorial University of Newfoundland, 2001.

[3] P.F. Rizos, N. Aspragathos, A.D. Dimarogonas, Identification of crack location and magnitude in a cantilever beam from the vibration modes, *Journal of Sound and Vibration* 138 (3) (1990) 381–388.

[4] B.P. Nandwana, S.K. Maiti, Detection of the location and size of a crack in stepped cantilever beams based on measurements of natural frequencies, *Journal of Sound and Vibration* 203 (3) (1997) 435–446.

[5] T.D. Chaudhari, S.K. Maiti, A study of vibration of geometrically segmented beams with and without crack, *International Journal of Solids and Structures* 37 (2000) 761–779.

[6] D.K.L. Tsang, S.O. Oyadiji, A.Y.T. Leung, Dynamic analysis of a penny-shaped crack by the fractal-like finite element method, *Proceedings of the Fifth International Conference on Vibration*, Nanjing, China, September 2002, pp. 59–65.

[7] S. Chinchalkar, Determination of crack location in beams using natural frequencies, *Journal of Sound and Vibration* 247 (3) (2001) 417–429.

[8] W.M. Ostachowicz, M. Krawczuk, Vibration analysis of a cracked beam, *Computers and Structures* 77 (2) (1990) 327–342.

[9] S.P. Lele, S.K. Maiti, Modeling of transverse vibration of short beams for crack detection and measurement of crack extension, *Journal of Sound and Vibration* 257 (3) (2002) 559–583.

[10] C.G. Go, Y.S. Lin, Infinitely small element for dynamic problems of cracked beam, *Engineering Fracture Mechanics* 48 (4) (1994) 475–482.

[11] W. Dahmen, Wavelet methods for PDES, some recent develops, *Journal of Computational Applied Mathematics* 128 (2001) 133–185.

[12] Albert Cohen, *Numerical Analysis of Wavelet Methods*, North-Holland Press, Amsterdam, 2003.

[13] S. Jaffard, P. Laurengot, Orthonormal wavelets, analysis of operators, and applications to numerical analysis, in: C.K. Chui (Ed.), *Wavelets—A Tutorial in Theory and Applications*, Academic Press, New York, 1992, pp. 543–601.

[14] J. Ko, A.J. Kurdila, M.S. Pilant, A class of finite element methods based on orthonormal, compactly supported wavelets, *Computational Mechanics* 16 (1995) 235–244.

[15] G. Beylkin, R. Coifman, V. Rokhlin, Fast wavelet transforms and numerical algorithms I, *Communications on Pure and Applied Mathematics* 44 (1991) 141–183.

[16] C. Canuto, A. Tabacco, K. Urban, The wavelet element method: part I. Construction and analysis, *Applied and Computational Harmonic Analysis* 6 (1999) 1–52.

[17] C. Canuto, A. Tabacco, K. Urban, The wavelet element method: part II. Realization and additional features in 2D and 3D, *Applied and Computational Harmonic Analysis* 8 (2000) 123–165.

[18] J.X. Ma, J.J. Xue, S.J. Yang, Z.J. He, A study of the construction and application of a Daubechies wavelet-based beam element, *Finite Elements in Analysis and Design* 39 (10) (2003) 965–975.

[19] X.F. Chen, S.J. Yang, J.X. Ma, Z.J. He, The construction of wavelet finite element and its application, *Finite Elements in Analysis and Design* 40 (5–6) (2004) 541–554.

[20] M.I. Friswell, J.E.T. Penny, The practical limits of damage detection and location using vibration data, *Proceedings of the 11th VPI and SU Symposium on Structural Dynamics and Control*, Blacksburg, 1997, pp. 31–40.

[21] I. Daubechies, Orthonormal bases of compactly supported wavelets, *Communications on Pure and Applied Mathematics* 41 (1988) 909–996.

[22] P.F. Rizos, N. Aspragathos, A.D. Dimarogonas, Identification of crack location and magnitude in a cantilever beam from the vibration modes, *Journal of Sound and Vibration* 138 (3) (1990) 381–388.

[23] A.D. Dimarogonas, Vibration of cracked structures: a state of the art review, *Engineering Fracture Mechanics* 55 (5) (1996) 831–857.

[24] G.M. Owolabi, A.S.J. Swamidas, R. Seshadri, Crack detection in beams using changes in frequencies and amplitudes of frequency response functions, *Journal of Sound and Vibration* 265 (2003) 1–22.
[25] J.T. Kim, N. Stubbs, Crack detection in beam-type structures using frequency data, *Journal of Sound and Vibration* 259 (1) (2003) 145–160.
[26] R.D. Adams, P. Cawley, C.J. Pye, B.J. Stone, A vibration technique for non-destructively assessing the integrity of structures, *Journal Mechanical Engineering Science* 20 (2) (1978) 93–100.
[27] J.N. Reddy, *An Introduction to the Finite Element Method*, McGraw-Hill Inc., New York, 1984.